RESEARCH ARTICLE | DECEMBER 18 2023

Modeling of electron refluxing and TNSA fields in laser–target interactions based on analysis of *Kα* emission

Eran Nardi ; Evgeny Stambulchik ; Zeev Zinamon; Yitzhak Maron

Phys. Plasmas 30, 123106 (2023)
https://doi.org/10.1063/5.0184656

Physics of Plasmas ARTICLE pubs.aip.org/aip/pop

Modeling of electron refluxing and TNSA fields in laser–target interactions based on analysis of $K\alpha$ emission

Cite as: Phys. Plasmas **30**, 123106 (2023); doi: 10.1063/5.0184656
Submitted: 26 October 2023 · Accepted: 6 December 2023 ·
Published Online: 18 December 2023

Eran Nardi,[a] Evgeny Stambulchik, Zeev Zinamon, and Yitzhak Maron

AFFILIATIONS

Faculty of Physics, Weizmann Institute of Science, Rehovot 7610001, Israel

[a]Author to whom correspondence should be addressed: eran.nardi@weizmann.ac.il

ABSTRACT

We analyze and model fast-electron-induced $K\alpha$ emission from an experiment in which a high-intensity ultra-short laser irradiated foil and bulk titanium targets. The motion of electrons inside the targets is calculated allowing for multiple scattering and collisional energy loss, while outside the target, electric fields of arbitrary configurations are assumed. It is shown that both the radial $K\alpha$-intensity distributions and the somewhat non-intuitive dependence of the absolute $K\alpha$ emission on the target thickness can be reproduced by taking into account the fast-electron refluxing with an electric field configuration based on the target normal sheath acceleration model. We infer the presence of a sheath electric field on the order of TV/m, extending to about 100μm in the radial direction. In addition, we obtain a temporal profile of the $K\alpha$ radiation.

I. INTRODUCTION

High-intensity ultra-short powerful lasers, when focused onto the surface of a solid target, generate an intense forward-moving electron beam of energies up to MeV's.[1,2] As the beam traverses the target, it produces a flux of x-ray radiation. Upon reaching the rear surface of the target, space-charge effects prevent majority of the electrons—except the most energetic ones—from leaving the target, thus causing the electrons to reflux. The refluxing has been studied experimentally by a considerable number of authors, such as Nersisyan *et al.*,[3] McKeever *et al.*,[4] Makita *et al.*,[5] Quinn *et al.*,[6] and Neumayer *et al.*[7] These studies have clearly established its existence and importance, in particular its influence on the radiation emission. A tightly related phenomenon is the formation of a sheath field that accelerates protons and other ions to MeV energies[8,9] through the target-normal-sheath-acceleration (TNSA) mechanism (e.g., see reviews of Badziak[10] and Macchi *et al.*[11]). We also note a recent study by Huang *et al.*[12] of hot refluxing electrons in a thin foil, with the dynamics governed by the spatiotemporal evolution of the self-generated sheath fields.

In this paper, we analyze the experimental data by Zastrau *et al.*[13] who provided radial distributions of $K\alpha$ emission from Ti foils of various thicknesses, as well as from a bulk Ti target, in an ultra-intense-laser–target interaction experiment. Notably, the radiation intensity from the thin, 10 μm foil was larger by factors of 1.5 and 3 than that from the 25 μm and bulk targets, respectively. It was also observed that the radial distribution of the $K\alpha$ radiation from the 10 and 25 μm foils is significantly broader than that from the bulk target. Here, these observations are reproduced with the fast-electron refluxing phenomenon accounted for, and bounds on the magnitude and spatial extent of the TNSA electric fields are obtained.

II. EXPERIMENTAL DATA USED

The laser energy on the target is 14 J, the pulse duration is 330 fs, the irradiation intensity at the fundamental laser frequency is $5 \times 10^{19}\mathrm{W/cm^2}$, and the laser spot size is 8μm.[13] 1D-resolved single-shot $K\alpha$ spectra are collected from the front side of the target at an angle of 50° to its normal. With the Abel transform applied, spectra at different radial positions are obtained. For the present study, total $K\alpha$ fluxes (i.e., these spectra integrated over the $K\alpha$ profile width) are used.

The relevant experimental data are presented in Fig. 1, where the radial $K\alpha$ flux distributions $I(r)$ of various target thicknesses are shown. These profiles can be roughly divided into three regions: the nearly-flat-top core (up to a few tens micrometer), the wing (up to $\sim 100\mu$m) characterized by a steep decrease in the intensity, and the slowly fading out halo extending further away.

The source of the $K\alpha$ halo, which makes up for about 30% of the total radiation, could be a low-energy isotropic electron emission.[4,5]

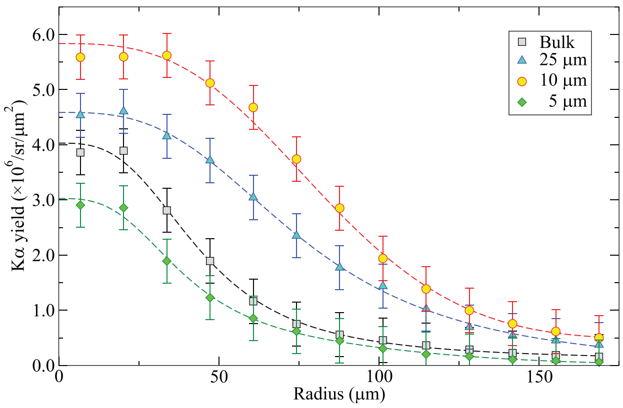

FIG. 1. Experimental data (adapted from Ref. 13). $K\alpha$ flux as a function of the radial coordinate for planar targets of various thicknesses.

The halo shape is rather similar for all target thicknesses, including the bulk target, as seen in Fig. 2, where ratios of the radially integrated $K\alpha$ flux $F(r)$ for different foil thicknesses to that of the bulk target are shown, with $F(r)$ defined as

$$F(r) = 2\pi \int_0^r r' dr' I(r'). \tag{1}$$

Thus, the focus of this study is on the central region (the core and the wing) that carries a more pronounced dependence on the target thickness and, therefore, provides a better sensitivity to the limited number of model parameters. Furthermore, the experimental uncertainties outside of this region become very large. It is also consistent with the previous analysis of a subset of the same data,[14] which succeeded in explaining heating of the core region.

III. NUMERICAL MODEL

The calculations of the fast electron trajectories within the solid titanium target accounted for collisional energy loss as well as for multiple scattering. The former process was calculated using the cold target

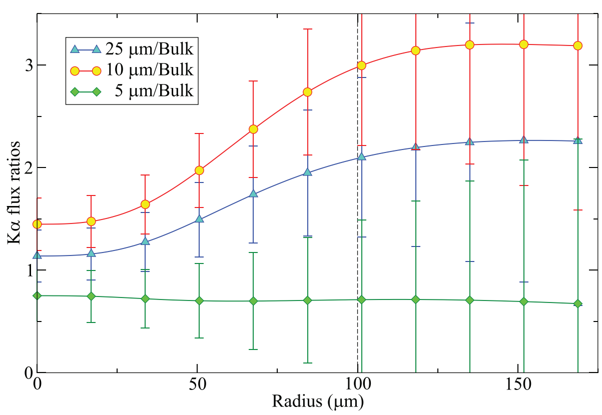

FIG. 2. Ratios of the radially integrated (from zero to a given radius) experimental $K\alpha$ intensity for different foil thicknesses vs that of the bulk target. The vertical dashed line designates an approximate beginning of the halo region.

dE/dx, since due to the relatively low temperatures attained in the experiment, plasma effects on the stopping can be neglected.[15] Multiple scattering was calculated using the Bethe–Molière theory[16] also assuming a cold target. For every segment of the electron path, the $K\alpha$ flux contribution in the direction of the detector was determined, with the dependence of the $K\alpha$ production on electron energy accounted for.[17] Importantly, self-absorption of $K\alpha$ photons as they make their way to the detector is included in the calculations, using the mean free path for $K\alpha$ absorption in titanium of about 20μm.[18] This value, which is on the order of the foil thicknesses used in the experiment, has an important bearing on the results.

A. Initial electron beam properties

In order to derive initial properties of the forward-moving intense electron beam, the experimental data obtained for the bulk target is used, where complex phenomena of electron refluxing do not exist. The three parameters of the model, governing the electron flow, are the effective emission spot size (limiting the area over which the electrons are accelerated at the target surface), the angular spread of the electron emission, and the fast-electron temperature T_{fast}. Gaussian-shaped radial and angular distributions are assumed with the standard deviations of R_b and ϕ_b, respectively.

The ballistic nature of the advancing electron beam is clearly seen in the experimental work and compilation of Green *et al.*,[19] where for the laser intensity of the experiment here discussed[13] the diverging angle is about 30°. Effective diverging angles of 24° and 16° at 4×10^{20} and $10^{19}\,\text{W/cm}^2$, respectively, have recently been measured.[20,21] A recent analysis[22] of bremsstrahlung data yields an incident electron angular spread of $15° \pm 8°$ at $2 \times 10^{19}\,\text{W/cm}^2$.

The electron energy spectrum was assumed to be Maxwellian with $T_{\text{fast}} = 1$ MeV. This value is between the ponderomotive and Beg values for the condition of the present experiment and agrees with the Beg-inspired fit of Lefebvre *et al.*[23] In addition, a recent bremsstrahlung experiment at similar conditions gave 1.1 MeV for the fast-electron temperature.[22] The back-scattered electrons, which constitute $\lesssim$20% in cold titanium targets at ambient conditions,[1] are assumed not to return to the target, even though restoring electric fields could develop on the front side of the target as here discussed.

In Fig. 3, the simulated radial intensity distribution of the $K\alpha$ radiation is compared to that of the experimental result of the bulk target, assuming angular beam divergences of 15° and 30°. The best fit for 15° is for the standard deviation of 36μm, while for the 30° case, it is 34μm. Both plots agree with the experiment within the range of experimental errors in the core part of the distribution. It is noted that the low-intensity "halo" is evident in the experimental data. As previously mentioned, in the analysis presented here this halo radiation is ignored.

B. Restoring electric fields

The forward-moving fast electrons exit the target and are emitted into the vacuum region at the back side of the foil, where they move in the electric field of the Debye sheath formed.[10,12,24] The electrons are returned to the foil, cross it in the opposite direction, and are emitted into the vacuum region at the front of the foil, whence they are returned into the target. This process is repeated several times with the

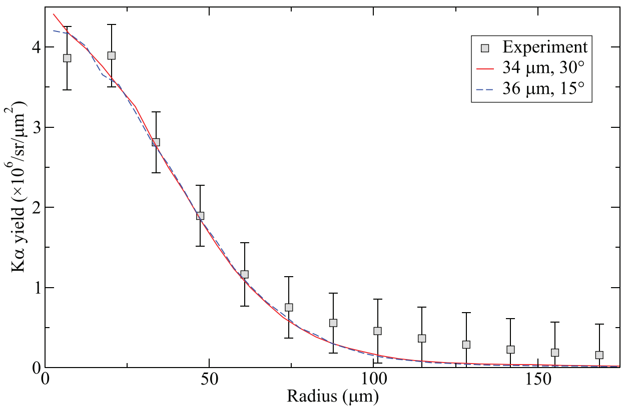

FIG. 3. Radial $K\alpha$ distribution in the bulk target. Comparison of the experimental data with two best-fit models.

electrons refluxing at the back and front sides of the foil and diffusing in the transverse direction until they exit the region of interest.[8]

In reality, the field configuration is of a complex nature.[25,26] However, in order to limit the number of free parameters in the model to a reasonable minimum, we follow the widely assumed approximation (e.g., see Markovits and Blaugrund,[27] Passoni and Lontano,[28] and Romagnani *et al.*[29]) that the electric field is normal to the foil. Denoting by z the distance from the edge of the foil, we write the restoring field $E(z)$ as[29]

$$E(z) = \begin{cases} E_0/(1+z/l_s), & z \geq 0, \\ 0, & z < 0, \end{cases} \tag{2}$$

where l_s is the Debye length of the sheath.[30] Based on the TNSA model,[8–10] we make use of a first-order relation between E_0 and l_s,

$$E_0 = kT_{\text{fast}}/(el_s), \tag{3}$$

where e is the elementary charge.

A temporal evolution of the electric-field magnitude is based on that given by Fuchs *et al.*,[31] in which the laser parameters are very similar to those in the experiment here analyzed.[13] Specifically, the field is assumed to be constant for the duration of the laser pulse (330 fs) and further decreasing as a Gaussian with the standard deviation $\sigma = 400$ fs.

In order to fit the experimental transverse radial emission profiles (which are much broader than that in the bulk target), a sheath of a considerable transverse extension is needed. We have found that a super-Gaussian flat-top distribution of order m, described by $\exp[-2(R/W)^m]$, gives a better fit to the experimental data than a Gaussian distribution. Here, R is the radial or transverse coordinate, and W is a measure of the width of the distribution. It was found that $W \simeq 100\mu$m (see Sec. IV) and $m = 9$ give satisfactory results.

It is assumed that the front-side field is the same as that at the back side of the foil. We have also tested the assumption that this field is half of that at the back of the foil, with only a moderate effect on the results. Some indications on the front-to-back electric-field ratios can be gained by comparison of thin foil backward to forward proton emission accelerated by these fields. Ceccotti *et al.*[32] find almost identical proton spectra from back and front of the target, but for ultrahigh-contrast laser pulses. In a lower contrast experiment,[33] it was found that the less abundant protons emitted from the back of the foil are of a higher average energy than the protons emitted from the front of the foil. The contrast of the laser pulse in the experiment analyzed here[13] lies in between these values.

As discussed in Sec. III A, the forward-moving fast electrons are injected into the foils with an angular spread of 15°. The electrons were emitted from a Gaussian spot size centered at $z = 0$, with a radius R_b. The initial electron energy distribution is Maxwellian with the temperature of 1 MeV. These three distributions (of the initial radial position, angle, and energy of the electron) are sampled by means of the Monte Carlo method. Each of the results given in Sec. IV is based on 15 000 events. An event is terminated when the electron exceeds the value of 80μm in the z axis direction or 250μm in the transverse direction.

In Fig. 4, we present typical calculated electron tracks for 10 and 25 μm foils, with the restoring field of 0.1TV/m (hence, $l_s = 10\mu$m) at both sides of the target. The electrons are emitted at 15° to the z axis from the origin ($z = 0$ and at $r = 0$) with the initial kinetic energy of 1 MeV. As seen in the figure, a few strong scattering events considerably distort the smooth appearances of the tracks. It is also observed that the electron distance in the vacuum region increases with the radial distance, since the restoring field is assumed to decrease with r.

Figure 4 also helps understanding why the radiation intensity from the 10 μm foil exceeds that of the thicker 25 μm one. Although in the case of the thinner foil, the electrons spend more time in the vacuum area, the induced $K\alpha$ emission from the target undergoes a significantly lesser absorption on the way to the detector (recall that the $K\alpha$ photon mean free path is about 20μm in solid titanium) than in the thicker, 25 μm foil.

IV. RESULTS AND DISCUSSION

The radial distribution of the $K\alpha$ emission for the 25, 10, and 5 μm foil targets and their ratios to the bulk $K\alpha$ yield are presented here.

The electron temperature of 1 MeV and the initial angular electron spread of 15° are used, as inferred from the bulk $K\alpha$ distribution (see Sec. III A). The three other parameters that influence the results are varied: the size of the initial radial distribution of the "hot"

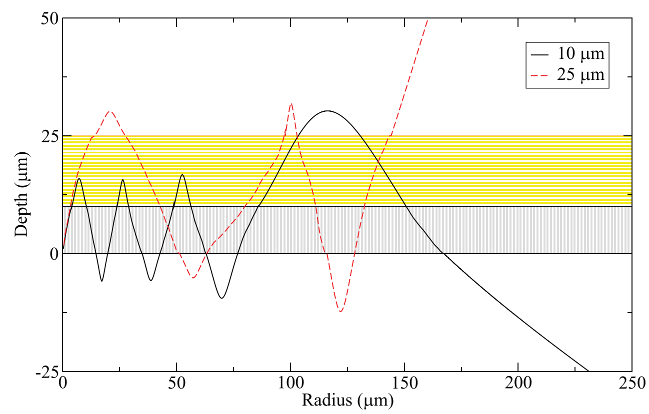

FIG. 4. Typical electron tracks, refluxing through a 10 or 25 μm foil. The targets are designated by the gray and yellow hashed areas, respectively.

electrons (R_b), the magnitude of the restoring electric field (E_0), and its radial extension (W).

Analysis of the 25 and 10 μm targets suggests a nearly identical set of the parameters providing best fit to the experimental results. In particular, $R_b = 60\mu$m is inferred. This is larger than $30 - 40\mu$m inferred for the bulk emission (see Fig. 3). The difference is attributed to the different conditions formed at the front surface of the bulk and foil targets. It is obtained that the value of W must be at least 125μm. $W = 150\mu$m gives the best fit, while larger yet values degrade the agreement slightly. This value significantly exceeds the estimate based on a single pass of the fast electrons,[31] even when allowing for a rapid traversal expansion of the sheath field.[25] As for E_0, the simulations suggest the values of a few TV/m, but in general, the results depend relatively weakly on the value of E_0 in excess of ~ 1 TV/m and nearly reach saturation at ~ 5 TV/m. The value and the geometry of the sheath electric field are comparable to those found in other studies. For example, while studying the bremsstrahlung emission, Chen and Sawada[34] found electric fields of up to 10 TV/m extending to radii of up to 500μm. Higher yet fields of 15 TV/m were also reported.[12] Lateral expansion of the electric field was also dealt with by McKenna *et al.*,[35] finding fields millimeters from the laser focus. In another study,[29] an order-of-magnitude lower electric field of ~ 0.5 TV/m was inferred; however, the irradiation intensity in that experiment, 10^{18}W/cm^2, was also significantly weaker.

A typical simulated radial $K\alpha$ distribution and its comparison with the experimental data are shown in Fig. 5(a). Figure 5(b) shows a detailed study of the 10 μm to bulk $K\alpha$ intensity ratios as a function of the radius. The results are given for different restoring fields E_0 with standard electron energy deposition (solid lines) as well as for the enhanced resistive stopping assumed (dashed lines). For the latter, the stopping is multiplied by a factor of 6 to account for increase in the stopping due to the intense return currents induced in the target, as it has previously been discussed.[14] The difference between the two approaches is very minor.[36] The reason for studying the intensity ratios as a function of R is to exclude the effect of the halo, which is observed in the experimental data, but not accounted for in the present theoretical modeling (see Fig. 3). In Fig. 5(b), the region where the halo begins to play an important role is indicated by the vertical dashed line. It is seen that except for the halo region, the agreement between the model and the experiment is very good for an electric field of $\gtrsim 5$TV/m assumed. We note that the range of the experimental uncertainties, indicated by the gray area in Fig. 5(b), is calculated assuming the worst-case scenario, i.e., that the error bars in Fig. 1 are all systematic and, thus, are accumulated by the integration in Eq. (1). It is believed that the true uncertainties are smaller.

A similar analysis of the 25 μm-foil results is given in Fig. 6. It is of interest to note that the $K\alpha$ flux in the 10 μm case is about 1.5 times larger than that of the thicker 25 μm foil. This non-intuitive result is due to the $K\alpha$ self-absorption effect within the target, as explained above in discussion of Fig. 4.

Thus, for both 10 and 25 μm targets, the electric field of a few TV/m extending over $\sim 100\mu$m radially is inferred. Contrary to the thicker targets, the 5 μm foil is very different, as seen in Fig. 7: a lower intensity and a significantly narrower distribution is evident. In these respects, it resembles the bulk target. Indeed, the radial distribution of the hot electrons with $R_b = 36\mu$m—the same as in the case of the bulk target—appears to explain the observed data best. The halo radiation is

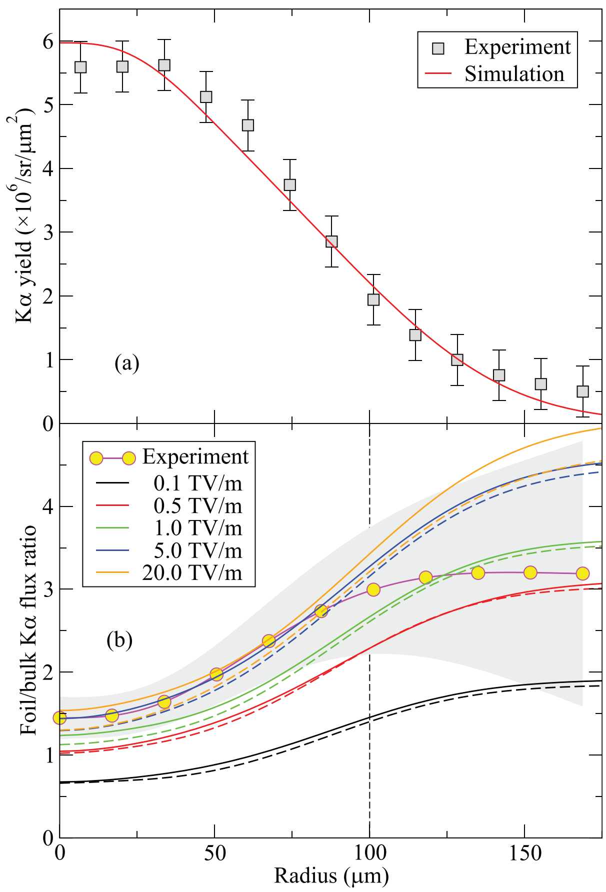

FIG. 5. (a) Radial distribution of the $K\alpha$ radiation from the 10 μm foil. $R_b = 60\mu$m, $E_0 = 5$TV/m, and $W = 150\mu$m assumed. (b) Foil-to-bulk $K\alpha$ ratio calculated for a few values of the restoring electric field E_0, indicated in the legend. The dashed lines correspond to the calculations performed assuming an enhanced resistive stopping (see the text). The vertical dashed line designates an approximate beginning of the halo region. The gray area represents the experimental uncertainties.

also very like that of the bulk target (while less prominent in the two other foil cases). Furthermore, the weaker intensity indicates a significantly lower, by two orders of magnitude, field, extending to a smaller area. It was suggested[13] that the distinct properties of the 5 μm target were due to a specific preplasma formation, since this specific foil was coated with 250 nm of copper. Alternatively, one can attribute these observations to a significant distortion of the target surfaces by a shock wave launched before the main laser pulse,[37] whereas in the case of the thicker targets, the TNSA sheath is formed before the slow moving shock wave reaches the rear side of the targets.

The present modeling allows for calculating the temporal shape of the $K\alpha$ radiation pulse, which is important in the context of using laser–matter interactions as intense ultra-fast radiation sources.[38,39] The temporal shapes of the $K\alpha$ pulses for different targets are shown in Fig. 8. The bulk case is the easiest to understand: while the fast electrons are supplied by the laser and propagate inside the target, creating K-shell holes along their paths, the number of $K\alpha$ photons increases.

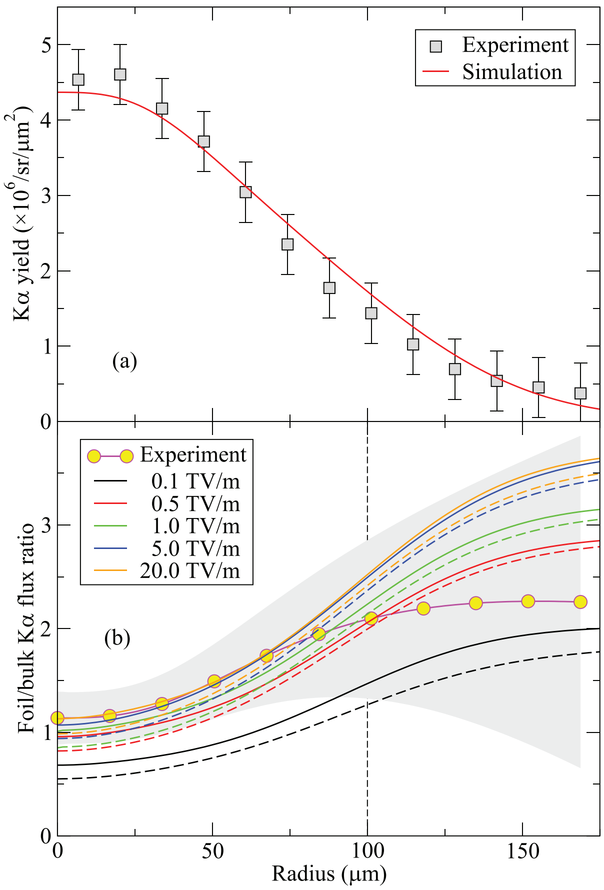

FIG. 6. Same as Fig. 5 ($R_b = 60\,\mu$m, $E_0 = 5$TV/m, and $W = 150\,\mu$m), but for the 25 μm target.

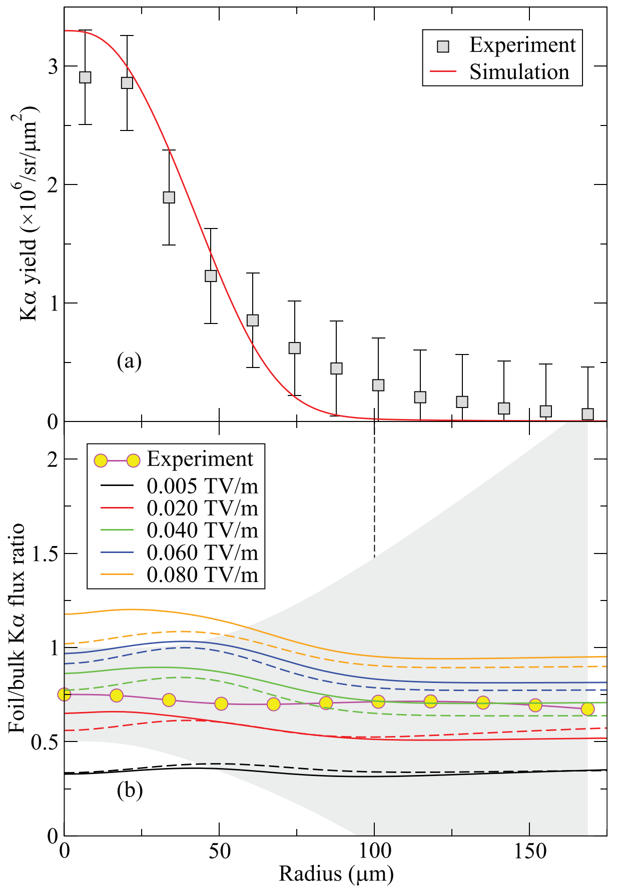

FIG. 7. (a) Radial distribution of the $K\alpha$ radiation from the 5 μm foil. $R_b = 36\,\mu$m, $E_0 = 0.04$ TV/m, and $W = 60\,\mu$m assumed. (b) Foil-to-bulk $K\alpha$ ratio calculated for a few values of the restoring electric field. The same notations as in Fig. 5(b).

As long as the electrons emitted at $t = 0$ do not deepen beyond the $K\alpha$ absorption length, i.e., during the first $\sim$70 fs, the growth is linear. Afterward, the growth rate slows down and the intensity approaches "saturation." At the end of the laser pulse ($t = 300$fs), the supply of the new fast electrons ends, while those previously emitted enter deeper yet target regions from which the number of $K\alpha$ photons reaching the observer decays exponentially. The shape resembles that of the capacitor voltage in a charge–discharge cycle, with the FWHM determined by the laser-pulse duration. The particle-in-cell simulations of Reich *et al.*,[40] when extrapolated to the irradiation intensities relevant for the present study, indicate that 90% of the $K\alpha$ pulse energy is emitted over about 1–2 ps, reasonably close to our result.

The shape of the $K\alpha$ pulse in the case of the 25 μm target closely matches that of the bulk target for the first $\sim$100 fs, including the beginning of the saturation phase. At this point, however, the initially injected electrons reach the rear target side and begin their way back. As a result, the radiation intensity returns to the linear growth. The electrons continue bouncing off the restoring fields at both sides of the target (see Fig. 4), forming the clearly seen "ripples" with the period of

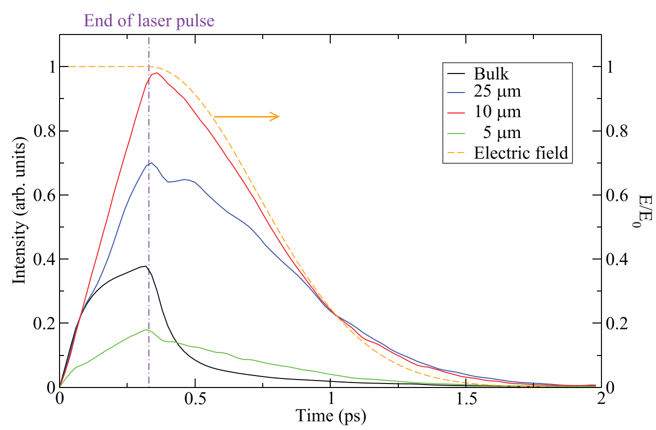

FIG. 8. Temporal shapes of the $K\alpha$ radiation from different targets. Also shown (the dashed line) is the electric field evolution assumed in the modeling of the foil targets. For the 25 and 10 μm foils, $E_0 = 5$ TV/m; for the 5 μm foil, $E_0 = 0.04$ TV/m. The vertical dot-dashed line indicates the end of the laser pulse.

$2d/c \approx 170$fs, decaying in time due to the electron scattering and energy spread. As the laser pulse switches off, the radiation intensity begins to decrease due to an increasing fraction of fast electrons overcoming the weakening field and leaving the target forever.

The case of the 10 μm target is similar, except that, due to the smaller thickness, the photon attenuation is much weaker, while the bouncing is 2.5 times faster. As a result, the ripples are nearly invisible. Finally, due to the much weaker fields formed at the surfaces of the 5 μm target, the fast electrons spend a significant time, about 300 fs, in the vacuum before returning to the foil. This results in a reduced $K\alpha$ yield compared to the other foil targets. Evidently, the duration of the $K\alpha$ pulse in the case of foil targets (about 1 ps) strongly depends on the electric-field evolution assumed in the model.[31] An experimental investigation of the $K\alpha$ duration by Nilson *et al.*[41] determined a few times longer pulses. However, limited-mass targets were used in that study, which might be responsible for extended electron rebouncing times.

The modeling predicts a near uniformity of the $K\alpha$ emissivity inside the target along the z direction. However, a larger x-ray flux near the front target surface was reported, for example, by Seely *et al.*[42] and Langhoff *et al.*[43] Novel tomographic experiments[44] are expected to provide accurate data on the z-dependence of the $K\alpha$ emissivity.

V. CONCLUSIONS

A model simulating $K\alpha$ emission resulting from the laser-induced electron beam interacting with planar foil and bulk titanium targets is constructed. The motion of the fast electrons inside the targets is calculated allowing for multiple scattering and collisional energy loss, while outside, it is governed by electric fields. For the latter, the TNSA theory is used as a framework for the present modeling, with the electron refluxing being key to the quantitative determination of the $K\alpha$ intensity ratios. Previously reported experimental results, where various targets were exposed to a $5 \times 10^{19}\mathrm{W/cm^2}$ laser radiation, are analyzed. An electric field of $\gtrsim 1\mathrm{TV/m}$, radially extending over $\sim 100\mu\mathrm{m}$, is inferred when the 10 and 25 μm-thick targets were used. However, in the case of the thinner 5 μm foil, a much weaker field appears to be formed, probably due to a strong deformation of the target by the shock wave. Notably, the effective size of the fast-electron-beam source in the 5 μm-foil case is the same as that of the bulk target ($R_b \approx 35\mu\mathrm{m}$), whereas for the thicker foils, it is about twice larger. In addition, we simulate temporal profiles of the $K\alpha$ radiation for all targets used in the experiment.

ACKNOWLEDGMENTS

This work was supported in part by the German–Israeli Foundation for Scientific Research and Development (GIF).

AUTHOR DECLARATIONS

Conflict of Interest

The authors have no conflicts to disclose.

Author Contributions

Eran Nardi: Conceptualization (equal); Formal analysis (equal); Investigation (equal); Methodology (equal); Software (equal); Validation (equal); Visualization (equal); Writing – original draft (equal); Writing – review & editing (equal). **Evgeny Stambulchik:** Conceptualization (equal); Formal analysis (equal); Investigation (equal); Methodology (equal); Validation (equal); Visualization (equal); Writing – original draft (equal); Writing – review & editing (equal). **Zeev Zinamon:** Conceptualization (supporting); Formal analysis (supporting); Investigation (equal); Methodology (equal); Writing – original draft (supporting). **Yitzhak Maron:** Conceptualization (supporting); Funding acquisition (lead); Project administration (lead); Writing – review & editing (supporting).

DATA AVAILABILITY

The data that support the findings of this study are available from the corresponding author upon reasonable request.

REFERENCES

[1] J. R. Davies, A. R. Bell, M. G. Haines, and S. M. Guérin, "Short-pulse high-intensity laser-generated fast electron transport into thick solid targets," Phys. Rev. E **56**, 7193–7203 (1997).

[2] A. P. L. Robinson, D. J. Strozzi, J. R. Davies, L. Gremillet, J. J. Honrubia, T. Johzaki, R. J. Kingham, M. Sherlock, and A. A. Solodov, "Theory of fast electron transport for fast ignition," Nucl. Fusion **54**, 054003 (2014).

[3] G. Nersisyan, M. Makita, K. McKeever, T. Dzelzainis, S. White, E. Nedanovska, B. Kettle, R. Nicholl, G. Williams, D. Riley, and C. L. S. Lewis, "Electron refluxing and K-shell line emission from Ti foils irradiated with subpicosecond laser pulses at 527 nm," Phys. Rev. E **85**, 056415 (2012).

[4] K. McKeever, M. Makita, G. Nersisyan, T. Dzelzainis, S. White, B. Kettle, B. Dromey, M. Zepf, G. Sarri, D. Doria, H. Ahmed, C. L. S. Lewis, D. Riley, and A. P. L. Robinson, "Fast-electron refluxing effects on anisotropic hard-x-ray emission from intense laser-plasma interactions," Phys. Rev. E **91**, 033107 (2015).

[5] M. Makita, G. Nersisyan, K. McKeever, T. Dzelzainis, S. White, B. Kettle, B. Dromey, D. Doria, M. Zepf, C. L. S. Lewis, A. P. L. Robinson, S. B. Hansen, and D. Riley, "Fast electron propagation in Ti foils irradiated with sub-picosecond laser pulses at $I\lambda^2 > 10^{18}\mathrm{Wcm^{-2}}\mu\mathrm{m}^2$," Phys. Plasmas **21**, 023113 (2014).

[6] M. N. Quinn, X. H. Yuan, X. X. Lin, D. C. Carroll, O. Tresca, R. J. Gray, M. Coury, C. Li, Y. T. Li, C. M. Brenner, A. P. L. Robinson, D. Neely, B. Zielbauer, B. Aurand, J. Fils, T. Kuehl, and P. McKenna, "Refluxing of fast electrons in solid targets irradiated by intense, picosecond laser pulses," Plasma Phys. Controlled Fusion **53**, 025007 (2011).

[7] P. Neumayer, B. Aurand, M. Basko, B. Ecker, P. Gibbon, D. C. Hochhaus, A. Karmakar, E. Kazakov, T. Kühl, C. Labaune, O. Rosmej, A. Tauschwitz, B. Zielbauer, and D. Zimmer, "The role of hot electron refluxing in laser-generated K-alpha sources," Phys. Plasmas **17**, 103103 (2010).

[8] S. P. Hatchett, C. G. Brown, T. E. Cowan, E. A. Henry, J. S. Johnson, M. H. Key, J. A. Koch, A. B. Langdon, B. F. Lasinski, R. W. Lee, A. J. Mackinnon, D. M. Pennington, M. D. Perry, T. W. Phillips, M. Roth, T. C. Sangster, M. S. Singh, R. A. Snavely, M. A. Stoyer, S. C. Wilks, and K. Yasuike, "Electron, photon, and ion beams from the relativistic interaction of petawatt laser pulses with solid targets," Phys. Plasmas **7**, 2076–2082 (2000).

[9] S. C. Wilks, A. B. Langdon, T. E. Cowan, M. Roth, M. Singh, S. Hatchett, M. H. Key, D. Pennington, A. MacKinnon, and R. A. Snavely, "Energetic proton generation in ultra-intense laser–solid interactions," Phys. Plasmas **8**, 542–549 (2001).

[10] J. Badziak, "Laser-driven generation of fast particles," Opto-Electron. Rev. **15**, 1–12 (2007).

[11] A. Macchi, M. Borghesi, and M. Passoni, "Ion acceleration by superintense laser-plasma interaction," Rev. Mod. Phys. **85**, 751–793 (2013).

[12] L. G. Huang, M. Molodtsova, A. Ferrari, A. L. Garcia, T. Toncian, and T. E. Cowan, "Dynamics of hot refluxing electrons in ultra-short relativistic laser foil interactions," Phys. Plasmas **29**, 023102 (2022).

[13] U. Zastrau, P. Audebert, V. Bernshtam, E. Brambrink, T. Kämpfer, E. Kroupp, R. Loetzsch, Y. Maron, Y. Ralchenko, H. Reinholz, G. Röpke, A. Sengebusch, E. Stambulchik, I. Uschmann, L. Weingarten, and E. Förster, "Temperature and $K\alpha$-yield radial distributions in laser-produced solid-density plasmas imaged with ultra-high-resolution x-ray spectroscopy," Phys. Rev. E **81**, 026406 (2010).

[14]E. Nardi, Z. Zinamon, E. Stambulchik, U. Zastrau, E. Kroupp, I. Uschmann, G. G. Paulus, and Y. Maron, "Target heating in femtosecond laser–plasma interactions: Quantitative analysis of experimental data," Phys. Plasmas **28**, 023101 (2021).
[15]E. Nardi and Z. Zinamon, "Energy deposition by relativistic electrons in high-temperature targets," Phys. Rev. A **18**, 1246–1249 (1978).
[16]H. A. Bethe, "Molière's theory of multiple scattering," Phys. Rev. **89**, 1256–1266 (1953).
[17]X. Llovet, C. J. Powell, F. Salvat, and A. Jablonski, "Cross sections for inner-shell ionization by electron impact," J. Phys. Chem. Ref. Data **43**, 013102 (2014).
[18]B. L. Henke, E. M. Gullikson, and J. C. Davis, "X-Ray interactions: Photoabsorption, scattering, transmission, and reflection at $E = 50$–30,000 eV, $Z = 1$–92," At. Data Nucl. Data Tables **54**, 181–342 (1993).
[19]J. S. Green, V. M. Ovchinnikov, R. G. Evans, K. U. Akli, H. Azechi, F. N. Beg, C. Bellei, R. R. Freeman, H. Habara, R. Heathcote, M. H. Key, J. A. King, K. L. Lancaster, N. C. Lopes, T. Ma, A. J. MacKinnon, K. Markey, A. McPhee, Z. Najmudin, P. Nilson, R. Onofrei, R. Stephens, K. Takeda, K. A. Tanaka, W. Theobald, T. Tanimoto, J. Waugh, L. Van Woerkom, N. C. Woolsey, M. Zepf, J. R. Davies, and P. A. Norreys, "Effect of laser intensity on fast-electron-beam divergence in solid-density plasmas," Phys. Rev. Lett. **100**, 015003 (2008).
[20]M. Storm, A. A. Solodov, J. F. Myatt, D. D. Meyerhofer, C. Stoeckl, C. Mileham, R. Betti, P. M. Nilson, T. C. Sangster, W. Theobald, and C. Guo, "High-current, relativistic electron-beam transport in metals and the role of magnetic collimation," Phys. Rev. Lett. **102**, 235004 (2009).
[21]M. Coury, D. C. Carroll, A. P. L. Robinson, X. H. Yuan, C. M. Brenner, M. Burza, R. J. Gray, K. L. Lancaster, Y. T. Li, X. X. Lin, D. A. MacLellan, H. Powell, M. N. Quinn, O. Tresca, C.-G. Wahlström, D. Neely, and P. McKenna, "Injection and transport properties of fast electrons in ultraintense laser-solid interactions," Phys. Plasmas **20**, 043104 (2013).
[22]T. S. Daykin, H. Sawada, Y. Sentoku, F. N. Beg, H. Chen, H. S. McLean, A. J. Link, P. K. Patel, and Y. Ping, "Characterization of fast electron divergence and energy spectrum from modeling of angularly resolved bremsstrahlung measurements," Phys. Plasmas **25**, 123103 (2018).
[23]E. Lefebvre, L. Gremillet, A. Lévy, R. Nuter, P. Antici, M. Carrié, T. Ceccotti, M. Drouin, J. Fuchs, V. Malka, and D. Neely, "Proton acceleration by moderately relativistic laser pulses interacting with solid density targets," New J. Phys. **12**, 045017 (2010).
[24]D. R. Rusby, C. D. Armstrong, G. G. Scott, M. King, P. McKenna, and D. Neely, "Effect of rear surface fields on hot, refluxing and escaping electron populations via numerical simulations," High Power Laser Sci. Eng. **7**, e45 (2019).
[25]C. P. Ridgers, M. Sherlock, R. G. Evans, A. P. L. Robinson, and R. J. Kingham, "Superluminal sheath-field expansion and fast-electron-beam divergence measurements in laser–solid interactions," Phys. Rev. E **83**, 036404 (2011).
[26]A. C. L. Fontaine, C. Courtois, E. Lefebvre, J. L. Bourgade, O. Landoas, K. Thorp, and C. Stoeckl, "Effects of electron recirculation on a hard x-ray source observed during the interaction of a high intensity laser pulse with thin Au targets," Phys. Plasmas **20**, 123111 (2013).
[27]M. Markovits and A. E. Blaugrund, "Diagnostic methods for investigation of collective ion acceleration," J. Appl. Phys. **59**, 3017–3022 (1986).
[28]M. Passoni and M. Lontano, "One-dimensional model of the electrostatic ion acceleration in the ultraintense laser–solid interaction," Laser Part. Beams **22**, 163–169 (2004).
[29]L. Romagnani, J. Fuchs, M. Borghesi, P. Antici, P. Audebert, F. Ceccherini, T. Cowan, T. Grismayer, S. Kar, A. Macchi, P. Mora, G. Pretzler, A. Schiavi, T. Toncian, and O. Willi, "Dynamics of electric fields driving the laser acceleration of multi-MeV protons," Phys. Rev. Lett. **95**, 195001 (2005).
[30]M. Roth and M. Schollmeier, "Ion acceleration–target normal sheath acceleration," in *Proceedings of the CAS-CERN Accelerator School: Plasma Wake Acceleration*, Geneva, Switzerland, 23–29 November 2014, CERN Yellow Reports: School Proceedings, Vol. 1, edited by B. Holzer (2016), pp. 231–270.
[31]J. Fuchs, P. Antici, E. d'Humières, E. Lefebvre, M. Borghesi, E. Brambrink, C. A. Cecchetti, M. Kaluza, V. Malka, M. Manclossi, S. Meyroneinc, P. Mora, J. Schreiber, T. Toncian, H. Pépin, and P. Audebert, "Laser-driven proton scaling laws and new paths towards energy increase," Nat. Phys. **2**, 48–54 (2006).
[32]T. Ceccotti, A. Lévy, H. Popescu, F. Réau, P. D'Oliveira, P. Monot, J. P. Geindre, E. Lefebvre, and P. Martin, "Proton acceleration with high-intensity ultrahigh-contrast laser pulses," Phys. Rev. Lett. **99**, 185002 (2007).
[33]P. McKenna, K. W. D. Ledingham, J. M. Yang, L. Robson, T. McCanny, S. Shimizu, R. J. Clarke, D. Neely, K. Spohr, R. Chapman, R. P. Singhal, K. Krushelnick, M. S. Wei, and P. A. Norreys, "Characterization of proton and heavier ion acceleration in ultrahigh-intensity laser interactions with heated target foils," Phys. Rev. E **70**, 036405 (2004).
[34]L. Chen and H. Sawada, "Characterization of sub-picosecond laser-produced fast electrons by modeling angularly resolved bremsstrahlung measurements with 3D hybrid particle-in-cell code," Phys. Plasmas **29**, 093104 (2022).
[35]P. McKenna, D. C. Carroll, R. J. Clarke, R. G. Evans, K. W. D. Ledingham, F. Lindau, O. Lundh, T. McCanny, D. Neely, A. P. L. Robinson, L. Robson, P. T. Simpson, C.-G. Wahlström, and M. Zepf, "Lateral electron transport in high-intensity laser-irradiated foils diagnosed by ion emission," Phys. Rev. Lett. **98**, 145001 (2007).
[36]It should be mentioned that in the absolute units, the enhanced resistive stopping does have a significant effect (about factor of two), however, it is nearly the same factor for the bulk and foil targets, so the ratios remain nearly unaffected.
[37]S. Eliezer, S. V. Pinhasi, J. M. M. Val, E. Raicher, and Z. Henis, "Heating in ultraintense laser-induced shock waves," Laser Part. Beams **35**, 304–312 (2017).
[38]C. M. Brenner, S. R. Mirfayzi, D. R. Rusby, C. Armstrong, A. Alejo, L. A. Wilson, R. Clarke, H. Ahmed, N. M. H. Butler, D. Haddock, A. Higginson, A. McClymont, C. Murphy, M. Notley, P. Oliver, R. Allott, C. Hernandez-Gomez, S. Kar, P. McKenna, and D. Neely, "Laser-driven x-ray and neutron source development for industrial applications of plasma accelerators," Plasma Phys. Controlled Fusion **58**, 014039 (2016).
[39]J. Vyskočil, O. Klimo, and S. Weber, "Simulations of bremsstrahlung emission in ultra-intense laser interactions with foil targets," Plasma Phys. Controlled Fusion **60**, 054013 (2018).
[40]C. Reich, P. Gibbon, I. Uschmann, and E. Förster, "Yield optimization and time structure of femtosecond laser plasma $K\alpha$ sources," Phys. Rev. Lett. **84**, 4846–4849 (2000).
[41]P. M. Nilson, J. R. Davies, W. Theobald, P. A. Jaanimagi, C. Mileham, R. K. Jungquist, C. Stoeckl, I. A. Begishev, A. A. Solodov, J. F. Myatt, J. D. Zuegel, T. C. Sangster, R. Betti, and D. D. Meyerhofer, "Time-resolved measurements of hot-electron equilibration dynamics in high-intensity laser interactions with thin-foil solid targets," Phys. Rev. Lett. **108**, 085002 (2012).
[42]J. F. Seely, C. I. Szabo, P. Audebert, and E. Brambrink, "Energetic electron propagation in solid targets driven by the intense electric fields of femtosecond laser pulses," Phys. Plasmas **18**, 062702 (2011).
[43]H. Langhoff, B. T. Bowes, M. C. Downer, B. Hou, and J. A. Nees, "Surface energy transport following relativistic laser-solid interaction," Phys. Plasmas **16**, 072702 (2009).
[44]E. Stambulchik, E. Kroupp, Y. Maron, U. Zastrau, I. Uschmann, and G. G. Paulus, "Absorption-aided x-ray emission tomography of planar targets," Phys. Plasmas **21**, 033303 (2014).